Enhancement of thermal stability of *Bacillus subtilis* 168 glycosyltransferase YjiC based on PoPMuSiC algorithm and its catalytic conversion of rare ginsenoside PPD

Abstract

YjiC, a glycosyltransferase from *Bacillus subtilis* 168, has great promise for natural product biosynthesis due to its aglycon promiscuity. In this study, the K125I/N178I variant with target residues located away from the substrate binding site was selected based on PoPMuSiC algorithm prediction and combined mutagenesis. The melting temperature (T_m) and $t_{1/2}$ at 55 ℃ were increased by 7.2 ℃ and 18 min, respectively. Enzyme kinetic analysis revealed that the K_m value of K125I/N178I was reduced by 11.4% but had a 1.21-fold increase in catalytic efficiency. Analysis of thermal stability mechanisms through fluorescence spectroscopy, LigPlot+ and molecular dynamics (MD) simulation showed that the increase in hydrophobic interactions and reduced structural flexibility are the main determinant factors for improved thermal stability. Finally, a ginsenoside PPD transformation system coupling Bs-YjiC and sucrose synthase (SuSy) was established at 45 ℃ using sucrose as the sugar donor. The space-time yield (STY) of ginsenoside F12 (415 mg L^{-1} h^{-1}) was 1.3 times higher than in previous studies. This is the first report on engineered Bs-YjiC for thermal stability improvement by rational design in industrial production of rare ginsenosides.

Keywords: Glycosyltransferase Bs-YjiC; PoPMuSiC; Thermostability; Molecular

dynamics simulations; Ginsenoside PPD

Abbreviations used: Bs-YjiC, glycosyltransferase YjiC from *Bacillus subtilis* 168; PPD, protopanaxadiol; PPT, protopanaxatriol; T_m, melting temperature; K_m, Michaelis constant; MD, molecular dynamics; AtSuSy, Arabidopsis sucrose synthase; STY, space-time yield; UDP, Uridine diphosphate; UDPG, uridine diphosphate glucose; UGTs, uridine diphosphate-dependent glycosyltransferases; WT, wild-type; FEL, free energy landscape; PCA, Principal component analysis; MSM, Markov State Models; SASA, Solvent-accessible surface area; RMSD, Root mean square deviation; RMSF, Root mean square fluctuation.

Introduction

Ginsenosides, the main pharmacologically active ingredients in Panax ginseng, have various biological effects, such as anti-oxidation, anti-tumor, and anti-inflammatory activities [1, 2]. Based on their triterpenoid skeleton, ginsenosides are classified as protopanaxadiol (PPD) or protopanaxatriol (PPT) [3]. The structural diversity of ginsenosides can be significantly expanded by changing the amount, location, and type of sugar attached to aglycones through the change in glycosylation mode [4]. Rare ginsenoside Rh2 has inhibitory effects on various tumors and can antagonize drug side effects, protect machine cells and improve immunity. Ginsenoside F12 has been shown to exhibit high cytotoxic effects on various cancer cells.

Glycation is a key mechanism in the biosynthesis of natural products that can improve the solubility, stability and bioavailability by forming different glycosides [5,

6]. However, the chemical glycosylation reaction conditions of ginsenosides are harsh, and the structure and type of products are difficult to control [7]. With the development of green chemistry and sustainable chemistry, new enzymatic reaction media such as green solvents are expected to overcome the shortcomings of existing biocatalysts [8-10]. *In vitro* enzymatic glycosylation mediated by uridine diphosphate-dependent glycosyltransferases (UGTs) has been used to overcome these challenges [11]. However, glycobase donors such as Uridine diphosphate glucose (UDPG) are expensive and are rarely available in large quantities. Sucrose synthetase (SuSy) is a key biocatalyst that catalyzes the conversion of cheap sucrose and UDP into UDPG and fructose [12, 13].

Bs-YjiC, a powerful and versatile UGT that is found in *Bacillus subtilis* 168*,* can glycosylate 19 structurally diverse natural product precursors and form glycosides using UDPG as the sugar donor [14]. It can also catalyze continuous glycosylation of PPD and PPT to synthesize various rare and unnatural ginsenosides [15, 16]. Therefore, Bs-YjiC development will expand the structural and functional diversity of natural products, leading to development of new lead compounds. Currently, only the regional, stereospecific, and enzyme activities of BS-YjiC have been extensively studied. Ma et al. constructed a single-variant M315F using a semi-rational design, which successfully improved the regional selectivity for synthesis of Rh2 by YjiC (~99%), and blocked further glycosylation of C12-OH [17]. However, the thermal stability of Bs-YjiC has yet to be established.

Thermal stability, catalytic efficiency, and substrate specificity determines the

feasibility of industrial enzyme applications [18, 19]. High temperatures can improve the reaction rates, reduce microbial contamination and improve substrate solubility [20, 21]. Thermal stabilities of enzyme proteins can be improved by practical designs. For instance, substitution of N-terminal amino acids [22], introduction of disulfide bonds [23], fusion of self-assembled peptides [24], increase the number of salt bridges [25] or hydrogen bonds [26], number of proline [27] and hydrophobic protein interactions [28]. The PoPMuSiC-2.1 server [29] can be used to assess predictions through a five-fold cross-validation procedure, allowing rapid calculation of stability changes due to unit point mutations in a protein after removal of 10% outliers. It is also used to estimate the correlations between the optimality of each amino acid in a protein sequence and its structural stability.

In this study, glycosyltransferase BS-YjiC was cloned from *Bacillus subtilis* 168 and expressed in *E. coli* BL21 (DE3). Through PoPMuSiC free energy calculation, the amino acid mutation sites were selected, and the mutants with improved thermal stability successfully obtained. Finally, the mechanisms underlying high thermal stabilities of variants were investigated via structural analysis and molecular dynamics simulation. This study provides valuable information for thermal stability modification of other glycosyltransferases.

Materials and Methods

2.1. Materials and chemicals

Uridine diphosphate glucose (UDPG), UDP, Protopanaxadiol (PPD), and

ginsenoside Rh2 standards were sourced from Yuanye Biotechnology (Shanghai, China). Fast Site-Directed Mutagenesis Kits were obtained from Tiangen Biochemical Technology (Beijing, China). The other chemicals used in this study were analytical grade (Solarbio, Beijing, China). All primers were synthesized by Shanghai Sangong (Shanghai, China).

2.2. Heterogonous expressions and purification

Codon optimization of Bs-YjiC (NP_389104) and AtSuSy (NM_001036838) genes was performed to construct the recombinant vectors, pET28a-Bs-YjiC and pET32a-AtSuSy, respectively (Tsingke, Beijing). After sequencing for heterologous expressions, the recombinant plasmid was transformed into *E. coli* BL21 (DE3) (Solarbio, Beijing, China) [15, 17].

Recombinant strains were cultured in LB medium at 37 °C and 200 rpm until the absorbance (OD_{600}) was 0.6-0.8. Then, they were treated with IPTG (0.3 mM) to induce recombinant protein expressions. Recombinant strains were further incubated at 16 °C for 16-20 h. Cell cultures were centrifuged at 5000 g, 4 ℃ for 15 min to obtain the bacterial precipitates that were re-suspended in a lysis buffer solution containing 50 mM Tris-HCl, 25 mM imidazole and 150 mM NaCl (pH 8.0) and crushed with an ultrasonic crushing instrument. Cellular extracts were centrifuged at 4 °C, 12,000 rpm for 1 h and the supernatants containing the crude enzyme solution obtained.

The prepared crude enzymes were purified using Ni-NTA agarose affinity column and eluted by 20-500 mM imidazole gradient. The pure proteins were dialyzed thrice

and concentrated. The purity and molecular weights of recombinant proteins were determined by SDS-PAGE gel electrophoresis. The Bradford method was used to determine protein concentrations. The molecular weights (Mw) and isoelectric points (pI) were predicted using ExPASy.

2.3. Construction of site-directed and combination variants

Site mutagenesis was conducted using a recombinant plasmid (pET28a-Bs-YjiC) with wild-type BS-YjiC as a template using a rapid site-specific mutation kit (Tiangen, Beijing). Variant plasmids were transformed into *E. coli* BL21 (DE3) cells after correct sequencing. The primers used for site-specific mutagenesis are shown in Table S1. Amino acid mutations at other sites were introduced to produce combination mutants using a positive variant as a template.

2.4. Enzyme activity assays

Enzymatic activities of BS-YjiC and its variants were conducted with 1 mM PPD, 4 mM UDPG, 50 mM Tris-HCl (pH 8.0), and a certain amount of enzymes. After incubation of the reaction systems at 40 ℃ for 30 min, the reactions were stopped by addition of equal volumes of methanol. The residual amounts of ginsenoside PPD were analyzed via the HPLC method.

Enzyme activities of AtSuSy were determined by 3,5-dinitrosalicylic acid colorimetry (DNS) [17]. The reactions were performed in a 500-μL reaction system containing 0.5 mM UDP, 300 mM sucrose, 50 mM Tris-HCl (pH 8.0) and various amounts of purified AtSuSy for 30 min at 40 ℃, then stopped in a boiling water bath

for 10 min. These assays were performed in triplicates.

2.5. Kinetic analysis of Bs-YjiC and its variants

Kinetic studies of PPD by Bs-YjiC and its variants were conducted as described in the enzyme activity assay. Briefly, 2 μg of purified enzyme protein, 50 mM Tris-HCl (pH 8.0), 10 mM $MgCl_2$, 10 mM UDPG and different concentrations of PPD (50-1000 μM) were incubated at 40 °C for 20 min. Then, the reactions were terminated by adding equal volumes of methanol. GraphPad Prism 9.0 was used to calculate the values of Mi constant (K_m) and maximum reaction rate (V_{max}). The predicted molecular weight of K_{cat} was 4.5×10^4 g/mol.

2.6 Assessment of thermostability

Residual activities of enzyme variants were measured by incubating the glycosyltransferase BS-YjiC variants at 45 ℃ for 90 min, cooling on ice for 10 min as described above and the enzyme activities measured.

Melting temperature (T_m) can also indicate proteomic thermal stability [30]. In this study, the T_m value was measured from a thermal gradient at 1 ℃/min by nanometer differential scanning calorimetry (DSC). Purified proteins were analyzed at a concentration of 0.25 mg/mL in 50 mM Tris-HCl buffer (pH 8.0), with the temperature increasing from 30 ℃ to 100 ℃.

2.7. Analysis of circular dichroism and surface hydrophobicity

Circular dichroism (CD) analysis was performed using a primary dichroism spectrometer (BRIGHTTIME Chirascan, Jasco-815). Enzyme ellipticity data were

continuously collected in the far-ultraviolet CD band from 190 to 260 nm at 4 °C using a 1 mm optical path quartz cuvette. Purified enzymes were dissolved in 50 mM Tris-HCl buffer (pH 8.0). The spectrum was averaged and corrected to determine the baseline contribution of the buffered solvent [31].

Surface hydrophobicity was determined using 1-aniline-8-naphthalene sulfate (ANS) as the fluorescence probe as described by Zhu et al. [32]. Fluorescence intensity was measured by fluorescence spectrophotometry (Hitachi-FL-1000, Japan). 0.4 mg/mL protein samples were diluted in 50 mM Tris-HCl buffer (pH 8.0), adding 10 μL ANS per 2 mL and excited at 317 nm. Emission spectra were recorded in a 1 cm cell at 300–500 nm.

2.8. Homology modeling, molecular docking, and molecular dynamics simulation

Homology modeling was performed using the Swiss-Model server [33] with the crystal structure (PDB ID: 6KQX) of YjiC from *Bacillus subtilis* as the template. The predicted structural model was verified by SAVES [34].

Protein-ligand docking was performed using AutoDock 4.2 [35]. A small molecule PPD was docked into the binding pocket of crystal structure 6KQX. The results were analyzed using PyMol 2.5 [36] to explain the high thermal stabilities of variants.

Molecular dynamics (MD) simulations were performed using GROMACS [37]. After processing the protein structure files for homology modeling into topology files, hydrogenation processing and selection of the appropriate force field for dynamics. Then, solvent water and ions were added to simulate the living environments of the

protein and were energy minimized. After equilibrating the temperature and pressure to bring the system to the desired equilibrium, the MD simulations were performed for 600 ns.

2.9 Optimization of reaction conditions for the variants/AtSuSy cascade

Different concentrations of UDP (0.1-0.4 mM), ginsenoside PPD (0.4-1.4 mM), sucrose (0.2-0.8 M), and DMSO (0-16%) were used in standard determination of cascade reactions to obtain the optimal concentrations. The effects of temperature (30-55 °C) and pH (6.5-8.5) on the reactions were also analyzed. Finally, the number of variants and AtSuSy was determined by adding different proportions of enzymes to the standard assay.

2.10 Fed-Batch synthesis of ginsenosides Rh2 and F12 via YjiC/AtSuSy cascade reaction

The variants/AtSuSy one-pot cascade was performed at 45 ℃ and 150 rpm based on the above optimization results. Briefly, PPD (100 μL, 200 mM) was added to 20 mL of the reaction mixture at 1, 2, 4, 6, 8, and 10 h, and 100 μL of reactant was collected and quenched by adding 4x the volume of methanol. Fresh enzymes were added at 4 and 8 h.

2.11 Chromatographic analysis of glycosylation products

HPLC and LC-MS were used to analyze the reactants. Briefly, the Diamonsil C18 (2) column (250 x 4.6 mm, 5 μm particles) was connected to the Shimadzu HPLC system for UV detection at 203 nm at 1 mL/min and at a column temperature of 35 ℃.

The column was eluted using solvents A (Water) and B (Acetonitrile) within 0-80 min using a gradient procedure of 30-55% B and within 60-100 min using 55-100% B. The LC-MS analysis was performed using Thermo Fly Ultimate 3000 UHPLC-Q Exactive (positive ion mode) with samples dissolved in methanol (Solarbio, Beijing, China).

3. Results and Discussion

3.1. Selection of variants with improved thermostability of BS-YjiC

3.1.1 Selection of key residues based on ΔΔGfold calculation

To improve the thermal stability of glycosyltransferase BS-YjiC, protein structure of wild-type (WT) YjiC was submitted to the PoPMuSiC algorithm tool for calculation. A smaller value of defolding free energy (ΔΔG) indicated that the variants were more stable than the WT [38]. Herein, 16 points with defolding free energy (ΔΔG) < -3.5 Kcal/mol were selected for experimental generation and testing (Table S2). After 90 min of incubation at 45 ℃, the K125I, N178I, and P313W variants retained 91.05%, 87.42%, and 89.48% residual activities. They were more resistant to heat treatment than WT. Besides, the initial enzyme activities did not decrease (Figure 1).

The K125I, N178I, and P313W variants were selected for combinatorial mutations to improve the thermal stability of glycosyltransferase BS-YjiC. Compared with the WT, initial enzyme activities of K125I/N178I and K125I/P313W variants were increased by 105.47% and 104.72%, respectively. And the residual activities after 90 min of incubation at 45 ℃ were 97.58% and 94.31%, respectively (Figure 2). Initial activities of the variants were also improved. Therefore, the K125I/N178I variants with

the best thermal stability were selected for subsequent analyses.

Li et al. [39] reported that beneficial amino acid mutations often exhibit cumulative or synergistic effects on thermal stabilities of proteins. In this study, the increased thermal stability of variant K125I/N178I denoted the feasibility of synergistic effects (Figures 1 and 2). Then, purified enzymes (K125I/N178I and WT) were heated at 55 °C with interval sampling in ice baths. It was found that WT had a $t_{1/2}$ of 21.27 min at 55 °C, while K125I/N178I had a $t_{1/2}$ of 39.28 min. Compared with WT, the K125I/N178I had 40% activity after 5 h of heating at 55 °C, and its $t_{1/2}$ increased by 18 min (Figure S4). Although the three residues (K125, N178, and P313) were located away from the substrate binding site, their mutual binding significantly improved the specific activities of the enzymes, suggesting that residues that do not form direct interactions with the substrate can also affect the enzyme activities of UGTs [40].

3.1.2 Kinetic parameters of combinational variants

Enzymatic properties of WT and variants were further studied. Compared with WT, the melting temperature (T_m) of all variants was higher. T_m of the combined variant K125I/N178I was increased by 7.2 ℃, whereas the optimal reaction temperature was increased by 5 ℃. These results suggest that substitutions of Lys125 and Asn178 significantly affected the enzymatic activities. The K_m value for K125I/N178I was 11.4% lower, relative to that of the WT (Table 1), indicating that variant K125I/N178I had a higher affinity for substrate ginsenoside PPD and its catalytic efficiency was significantly improved by 1.21 times.

3.2 Spectral characterization of the structure of BS-YjiC and variants

Proteins with different secondary structures resulted in CD profiles with different positions and strengths [41]. Figure S6 shows that variant K125I/N178I and the WT had the maximum negative peak at 195 nm and negative peaks at 208 nm and 222 nm, consistent with CD spectral characteristics of α-helix and β-sheet conformations. The trend of CD bands for K125I/N178I was comparable with that of WT, indicating that the mutation did not significantly change the secondary structure.

Increasing hydrophobic interactions by reducing hydrophobicity of the protein surface and enhancing hydrophobicity of residues inside the protein is an effective strategy for increasing protein stability [42]. Therefore, hydrophobicity and flexibility of WT and variant K125I/N178I were further analyzed.

Protein surface hydrophobicity was detected via the ANS hydrophobic fluorescence probe, which was bound to the non-polar region of the protein surface or membrane [43]. Compared with the WT, the fluorescence intensity for variant K125I/N178I was significantly reduced, indicating that surface hydrophobicity of the variant was also decreased (Figure 3). This may have resulted in a more compact structure of the whole protein.

Thermal stability of proteins is positively correlated with hydrophobicity of internal residues and negatively correlated with flexibility [44]. The hydrophobicity and flexibility for WT and variant K125I/N178I were initially characterized using the online software, ProtScale [45]. Substitution of residues Lys125 and Asn178 increased

the hydrophobicity and decreased the flexibility in 124-126 and 177-179 regions, respectively (Figure 4). Therefore, improved thermostability for variant K125I/N178I is associated with increased hydrophobicity of internal residues and decreased flexibility within the protein.

3.3 Molecular mechanisms in enhanced thermostability of BS-YjiC

3.3.1 Homology modeling

The structural model was constructed using the Swiss-model server with the structure (PDB ID: 6KQX) of BS-YjiC as the template. The QMEAN Z-Score for the predicted structure was -1.42. YjiC adopts the classical GT-B fold (Figure 5), consisting of two Rossman-like β/α/β fold domains [46]. The RC plots were used to assess the structural models of the WT and its variants (Figure S8). These results suggest that the predicted models can be used for molecular docking and MD analysis.

3.3.2 Molecular docking and molecular dynamics study of complexes

The 6KQX structure with small molecule UDP was used as a reference to connect the small molecule PPD into the binary complex using Autodock (Figure 5). The PPD and UDP were bound to N-terminal (residues 6-199) and C-terminal domains (residues 222-387) of YjiC, respectively, while the mutation sites (Lys125 and Asn178) were in two adjacent β-sheets away from the substrate binding site. The LigPlot+ [47] analysis revealed that the mutation had little effects on the substrate binding site, and both WT and mutant K125I/N178I exhibited 8 hydrophobic interaction forces, 3 hydrogen bonds with ginsenoside PPD, 6 hydrophobic interaction forces and 14 hydrogen bonds with

UDP (Figure 6). The hydrophobic interactions with Glu175 and Cys127 were increased near Lys125 and Asn178, respectively. In addition, hydrophobic interactions between Lys125 and Asn178 may be responsible for the synergistic effects [48].

Interactions between the enzyme and ligand can significantly affect the catalytic activities, substrate-binding affinity, and enzyme stability [49]. The MD simulation of the pure protein and ligand was performed at 1 ps. It was found that the purified protein and ligand steadily fluctuated at 1.5 Å and 3 Å (Figure S9). Then, MD simulation of the complex was performed within 100 ns. The RMSD value of the ligand exhibited a continuous increase at 40 ns and 75 ns, indicating that the ligand had moved away from the binding site and eventually away from the protein itself [50]. However, the mutant and ligand have better binding conditions. In Amber 22, molecular mechanics/Poisson-Boltzmann surface area calculations using MMPBSA.py revealed the energy distribution of the proteins of the complex system to show the stability of the whole system [51]. The binding free energy (ΔG) for variant K125I/N178I to small molecules decreased to -76.91 kcal/mol, compared with the WT enzyme (-64.02 kcal/mol), indicating that the mutation resulted in a 1.2-fold increase in affinity of the enzyme to the substrate, consistent with results of enzyme kinetics.

The MD simulation trajectories were analyzed to determine the dynamic cross-correlations between residuals in the BS-YjiC structure. Regarding the correlated dynamic motions, a reciprocal correlation matrix was generated (Figure 7A) [52, 53].

The yellow blocks shown indicate residues with high correlation motions while the blue blocks indicate minimal correlations. Residues in the variant-ligand complex exhibited higher correlations and similarity to the pure protein. The free energy landscape (FEL) indicates protein folding reaching a minimum energy state [54, 55]. Relative stabilities of the WT and mutant K125I/N178I structures can be quantitatively estimated by Boltzmann inversion calculation of the two-dimensional probability distribution of the corresponding reaction coordinates. Comparisons of FEL for pure protein, WT-ligand complexes, and variant-ligand complexes revealed that the variants had better changes in conformational stability (Figure 7B).

The Markov State Model (MSM) is an accurate approach for summarizing the equilibrium of conformational ensembles and can explain the biological mechanisms [56]. Macrostate MSM has been successfully used in studies of functional conformational changes of various proteins through the dynamic set method [57]. An MSM of 1 μs is constructed based on free energy landscape parameters, after which the properties of Markov quantities are verified by calculating the transformations between different macrostate conformations [58]. In figure 8, conformation 8 was the main macroscopic state, accounting for 35% of the entire simulation. Transition times from conformation 7→8, 6→8, and 4→8 were significantly shorter than those of other conformations. Principal component analysis (PCA) was performed to explain the scattering trajectory of amino acid residues due to changes in protein structures. In the PC1 mode, characteristic vectors of the trajectory were better, becoming the global

motion of the trajectory (Figure S10).

Allosteric residues were investigated starting from the typical protein macrostructure by binding the docking complex of pure WT protein and variant [48]. The ligands propagated allosteric effects to distal sites via proximal sites, such as S82 →K78 and Y125→T316→Q313→Y311 (Figure S11). Studies have shown that distal mutations easily enhance the enzyme activity, and most of the modifications that improved the activity were located on the coil [59, 60].

3.3.3 Molecular dynamics of Bs-YjiC and its variants

To further explain the effect of thermal stability on protein folding, molecular dynamics simulations at 600 ns were performed at different temperatures (308 K, 400 K, 440 K, and 480 K) until the unfolding process was observed to identify significant conformational changes. The thermomolecular mechanism of the WT and its variants (K125I, K125I/N178I and M315F) on structural stability was also explored.

Solvent-accessible surface area (SASA) reflects protein hydrophobicity [61, 62]. Improving the overall hydrophobicity of the protein is conducive to its internal folding, thereby improving its stability. In this study, SASA of the four proteins exhibited the same trend over time at different temperatures (Figure 9). At 480 K, the mean SASA for variant K125I/N178I decreased to 177.40 while that of the WT was 200.17, suggesting that mutations at Lys125 and Asn178 inhibited the interactions between BS-YjiC and water molecules, increasing protein compaction.

Root mean square deviation (RMSD) can be used to estimate the thermal

fluctuation of protein conformations. The RMSD values for proteins are negatively correlated with their thermal stability and positively correlated with their rigidity [63]. The protein structure progressively became unstable as the temperature increased, which led to significant fluctuations in the corresponding RMSD curve (Figure 10). Compared with other variants, mean RMSD values for variant K125I/N178I were slightly lower than those of other enzymes at 440 K and 480 K. Thus, variant K125I/N178I had better thermal stability at high temperatures than the WT.

Root mean square fluctuation (RMSF) value reflects the freedom and flexibility of the residue in the protein structure [64]. Figure 11 shows that residues in regions 127-177 belonging to coils were more flexible and caused larger fluctuations. Overall fluctuations for variants RMSF at 308 K and 400 K were similar to those of WT. The RMSF value at 440 K was higher in K125I than in the WT (260-280 residues). Compared with the WT, the RMSF values for variant K125I/N178I at 480 K were significantly reduced in 90-135 and 155-180 regions. Most changes occurred in the loop region. Mutation residues for Lys125 and Asn178 were located in β-sheet, as revealed by cyan sticks in Figure 5. There was reduced amino acid flexibility at both terminals of the coils region, which greatly promoted thermal stability of BS-YjiC. The RMSF values for K125I/N178I were significantly increased in the 227-250 region, indicating that coil structures at both ends of the helix (234-245) were more unstable at high temperatures, which may be an adverse effect of the distal impact on UDP binding region [48].

Thermosensitive residues of proteins and their positions can be identified by differences in their RMSF values [65]. The RMSF difference analysis revealed that the mutant K125I/N178I had the least thermosensitive residues, while the Asn178 and Lys125 sites had synergistic effects, where one site caused the adjacent residues (underlined region) of the other site to change from thermally sensitive to thermally stable residues (Table S3). Mutations in Asn178 and Lys125 sites also increased the heat-sensitive residues in the 230-251 region. However, mutant M315F had increased heat-sensitive residues, consistent with optimal temperatures decreasing to 35 ℃ in the study by Ma et al. [17].

The evolution of secondary structures related to structural flexibility was further studied [66]. Secondary structures of the wild type, K125I and M315F began to show obvious fluctuations at 440 K, with the α-helix, β-fold, and 3-helix becoming less stable and unfolding (Figures S12 and S13). The α-helix had the highest contribution to the whole secondary structure. The secondary structure for K125I/N178I remained stable, compared to other enzymes in all studied temperatures. Therefore, mutations at Lys125 and Asn178 sites slightly increased the stability of the secondary structures of enzymes. In summary, by simulating the conformational change of the enzyme under conditions closest to the experimental environment, the constant change of each atom in the protein with temperature is predicted, thus revealing the positive effect of the increase in hydrophobic interaction forces and structural tightness on the thermal stability of the protein structure.

3.4 Construction of a one-pot cascade catalytic system with the variant and AtSuSy

3.4.1 Reaction optimization for PPD conversion

The one-pot K125I/N178I-AtSuSy double enzyme coupled glycosylation PPD conversion system containing sucrose as a sugar donor and UDP-glucose recycling can efficiently and economically produce rare ginsenosides, F12 and Rh2. When sufficient AtSuSy was provided, the maximum yield for ginsenoside Rh2 was obtained with addition of 100 mU/mL mutase K125I/N178I, and conversion of ginsenoside PPD was only slightly increased with continued addition of the mutant enzyme (Table 2). When the AtSuSy concentration was increased from 60 mU/mL to 360 mU/mL, the conversion of ginsenoside PPD was increased from 25% to 73%. However, the production of ginsenoside Rh2 was minimized with addition of 240 mU/mL AtSuSy, indicating that sufficient UDPG was provided for continuous glycosylation reactions at this time. Therefore, the optimal addition amounts of Bs-YjiC and AtSuSy were 100 mU/mL and 240 mU/mL, respectively.

The optimal reaction conditions were further determined at different temperatures (30-55 ℃), pH levels (6.5-8.5), DMSO concentration (0-16%), and sucrose concentration (0.2-0.8 M). The highest conversion of PPD was obtained at 45 ℃, pH 8.0, 6% DMSO, and 0.5 M sucrose (Figure 12). Continued optimization of reaction concentrations of UDP (0.1-0.4 mM) and PPD (0.4-1.4 mM) in the reaction as the key cofactors and substrates in the cascade is crucial since UDP and PPD have complex effects on UGT activities. The conversion rate of PPD increased by 1.46 times at 0.25

mM UDP, while the conversion rate of PPD slightly decreased with increasing UDP concentration, indicating that the high UDP concentration inhibited PPD glycosylation. The conversion decreased from 97% to 51% when PPD concentration increased from 0.4 mM to 1.4 mM. The maximum ginsenoside F12 yield (0.74 mM) was obtained at 1.0 mM PPD. Finally, fed-batch reactions were performed at 45 ℃, pH 8.0, 6% DMSO, 0.25 mM UDP, 0.5 M sucrose, and 1.0 mM PPD.

3.4.2 Process optimization with substrate PPD fed-batch strategy

The substrate feeding strategy was adopted to prepare rare ginsenosides by regularly adding PPD in the batch reaction based on optimized reaction conditions while avoiding the inhibitory effects of the substrate or product. The UGTs rapidly reacted within the first hour, almost completely converting 1 mM PPD to 0.02 mM ginsenoside Rh2 and 0.94 mM F12 (Figure 13). Ginsenoside F12 was the main product of the cascade reaction, with only a trace amount of ginsenoside Rh2, consistent with *in vitro* enzymatic reactions of UDPG as a glucose donor (Figure S15). However, increased initial PPD concentration at 10 h decreased the contents of the intermediate product Rh2 and final product F12 in the reaction system, the consumption of enzymes and reduced the reaction rate to 30.06%. At 14 h, PPD (7 mM) produced 0.39 mM ginsenoside Rh2 (0.24 g/L) and 6.54 mM ginsenoside F12 (5.13 g/L) with a conversion rate of 93%. The yield of ginsenoside F12 within 12 h (415 mg L^{-1} h^{-1}) was 1.3 times that reported by Dai et al. (332 mg L^{-1} h^{-1}) [15].

4. Conclusions

In this study, variants with improved thermal stability were predicted and obtained by defolding free energy (ΔΔG) calculation. Through secondary structure, molecular docking, molecular dynamics, and three-dimensional structure analyses, it was found that the increase in hydrophobic interaction forces and the decrease in structural flexibility for mutant K125I/N178I were the main reasons for its improved thermal stability. Ginsenoside F12 (5.13 g/L) and Rh2 (0.24 g/L) were obtained by efficiently converting ginsenoside PPD through *in vitro* glycosylation with double enzyme coupling. The temporal and space-time yield (STY) for ginsenoside F12 was 1.3 times higher than that reported in previous studies. To the best of our knowledge, this is the first time that the thermal stability for glycosyltransferase BS-YjiC has been modified, which is a potential strategy for thermal stability engineering of glycosyltransferase.

References

[1] L. Li, S.Y. Shin, S.J. Lee, J.S. Moon, W.T. Im, N.S. Han, Production of Ginsenoside F2 by Using Lactococcus lactis with Enhanced Expression of beta-Glucosidase Gene from Paenibacillus mucilaginosus, J Agric Food Chem 64(12) (2016) 2506-2512.

[2] P. Wang, W. Wei, W. Ye, X. Li, W. Zhao, C. Yang, C. Li, X. Yan, Z. Zhou, Synthesizing ginsenoside Rh2 in Saccharomyces cerevisiae cell factory at high-efficiency, Cell Discov 5 (2019) 5.

[3] F. Jiang, C. Zhou, Y. Li, H. Deng, T. Gong, J. Chen, T. Chen, J. Yang, P. Zhu, Metabolic engineering of yeasts for green and sustainable production of bioactive ginsenosides F2 and 3beta,20S-Di-O-Glc-DM, Acta Pharm Sin B 12(7) (2022) 3167-3176.

[4] H. Liang, Z. Hu, T. Zhang, T. Gong, J. Chen, P. Zhu, Y. Li, J. Yang, Production of a bioactive unnatural ginsenoside by metabolically engineered yeasts based on a new

UDP-glycosyltransferase from Bacillus subtilis, Metab Eng 44 (2017) 60-69.

[5] Y. Zhuang, G.Y. Yang, X. Chen, Q. Liu, X. Zhang, Z. Deng, Y. Feng, Biosynthesis of plant-derived ginsenoside Rh2 in yeast via repurposing a key promiscuous microbial enzyme, Metab Eng 42 (2017) 25-32.

[6] A. Gutmann, A. Lepak, M. Diricks, T. Desmet, B. Nidetzky, Glycosyltransferase cascades for natural product glycosylation: Use of plant instead of bacterial sucrose synthases improves the UDP-glucose recycling from sucrose and UDP, Biotechnol J 12(7) (2017) 1600557.

[7] B. Fan, T. Chen, S. Zhang, B. Wu, B. He, Author Correction: Mining of efficient microbial UDP-glycosyltransferases by motif evolution cross plant kingdom for application in biosynthesis of salidroside, Sci Rep 7(1) (2017) 17147.

[8] W. Yang, J. Zhou, Q. Gu, J.D. Harindintwali, X. Yu, X. Liu, Combinatorial Enzymatic Catalysis for Bioproduction of Ginsenoside Compound K, J Agric Food Chem (2023) 101449.

[9] W. Yang, Q. Gu, J. Zhou, X. Liu, X. Yu, High-Value Bioconversion of Ginseng Extracts in Betaine-Based Deep Eutectic Solvents for the Preparation of Deglycosylated Ginsenosides, Foods 12(3) (2023) 496.

[10] W. Yang, J. Zhou, Q. Gu, J. Zhang, J.D. Harindintwali, X. Liu, X. Yu, Identification of nutritional values of the fermentative extract from the mixture of Stereum hirsutum mycelial substrates and ginseng extracts, Lwt 161 (2022) 113179.

[11] A. Geraldi, Ni'matuzahroh, Fatimah, C.-H. Cui, T.T. Nguyen, S.C. Kim, Enzymatic biotransformation of ginsenoside Rb1 by recombinant β-glucosidase of bacterial isolates from Indonesia, Biocatalysis and Agricultural Biotechnology 23 (2020) 101449.

[12] K. Schmolzer, M. Lemmerer, A. Gutmann, B. Nidetzky, Integrated process design for biocatalytic synthesis by a Leloir Glycosyltransferase: UDP-glucose production with sucrose synthase, Biotechnol Bioeng 114(4) (2017) 924-928.

[13] G. Dewitte, M. Walmagh, M. Diricks, A. Lepak, A. Gutmann, B. Nidetzky, T. Desmet, Screening of recombinant glycosyltransferases reveals the broad acceptor specificity of

stevia UGT-76G1, J Biotechnol 233 (2016) 49-55.

[14] L. Dai, J. Li, P. Yao, Y. Zhu, Y. Men, Y. Zeng, J. Yang, Y. Sun, Exploiting the aglycon promiscuity of glycosyltransferase Bs-YjiC from Bacillus subtilis and its application in synthesis of glycosides, J Biotechnol 248 (2017) 69-76.

[15] L. Dai, C. Liu, J. Li, C. Dong, J. Yang, Z. Dai, X. Zhang, Y. Sun, One-Pot Synthesis of Ginsenoside Rh2 and Bioactive Unnatural Ginsenoside by Coupling Promiscuous Glycosyltransferase from Bacillus subtilis 168 to Sucrose Synthase, J Agric Food Chem 66(11) (2018) 2830-2837.

[16] L. Dai, J. Li, J. Yang, Y. Zhu, Y. Men, Y. Zeng, Y. Cai, C. Dong, Z. Dai, X. Zhang, Y. Sun, Use of a Promiscuous Glycosyltransferase from Bacillus subtilis 168 for the Enzymatic Synthesis of Novel Protopanaxatriol-Type Ginsenosides, J Agric Food Chem 66(4) (2018) 943-949.

[17] W. Ma, L. Zhao, Y. Ma, Y. Li, S. Qin, B. He, Oriented efficient biosynthesis of rare ginsenoside Rh2 from PPD by compiling UGT-Yjic mutant with sucrose synthase, Int J Biol Macromol 146 (2020) 853-859.

[18] H. Chi, Y. Wang, B. Xia, Y. Zhou, Z. Lu, F. Lu, P. Zhu, Enhanced Thermostability and Molecular Insights for l-Asparaginase from Bacillus licheniformis via Structure- and Computation-Based Rational Design, J Agric Food Chem 70(45) (2022) 14499-14509.

[19] J. Guo, Y. Wang, X. Zhang, W. Gao, Z. Cai, T. Hong, Z. Man, Q. Qing, Improvement of the Catalytic Activity of Chitosanase BsCsn46A from Bacillus subtilis by Site-Saturation Mutagenesis of Proline121, J Agric Food Chem 69(40) (2021) 11835-11846.

[20] Y. Yang, L. Zhang, M. Guo, J. Sun, S. Matsukawa, J. Xie, D. Wei, Novel alpha-L-arabinofuranosidase from Cellulomonas fimi ATCC 484 and its substrate-specificity analysis with the aid of computer, J Agric Food Chem 63(14) (2015) 3725-3733.

[21] X. Li, X. Zhang, S. Xu, M. Xu, T. Yang, L. Wang, H. Zhang, H. Fang, T. Osire, Z. Rao, Insight into the thermostability of thermophilic L-asparaginase and non-thermophilic L-asparaginase II through bioinformatics and structural analysis, Appl Microbiol Biotechnol 103(17) (2019) 7055-7070.

[22] Y. Yang, J. Sun, J. Wu, L. Zhang, L. Du, S. Matsukawa, J. Xie, D. Wei, Characterization of a Novel alpha-l-Arabinofuranosidase from Ruminococcus albus 7 and Rational Design for Its Thermostability, J Agric Food Chem 64(40) (2016) 7546-7554.

[23] X. Ban, J. Wu, B. Kaustubh, P. Lahiri, A.S. Dhoble, Z. Gu, C. Li, L. Cheng, Y. Hong, Y. Tong, Z. Li, Additional salt bridges improve the thermostability of 1,4-alpha-glucan branching enzyme, Food Chem 316 (2020) 126348.

[24] P. Xu, Z.F. Ni, M.H. Zong, X.Y. Ou, J.G. Yang, W.Y. Lou, Improving the thermostability and activity of Paenibacillus pasadenensis chitinase through semi-rational design, Int J Biol Macromol 150 (2020) 9-15.

[25] X. Lu, J. Chen, L. Jiao, L. Zhong, Z. Lu, C. Zhang, F. Lu, Improvement of the activity of l-asparaginase I improvement of the catalytic activity of l-asparaginase I from Bacillus megaterium H-1 by in vitro directed evolution, J Biosci Bioeng 128(6) (2019) 683-689.

[26] Y. Hua, C. Lyu, C. Liu, H. Wang, S. Hu, W. Zhao, J. Mei, J. Huang, L. Mei, Improving the Thermostability of Glutamate Decarboxylase from Lactobacillus brevis by Consensus Mutagenesis, Appl Biochem Biotechnol 191(4) (2020) 1456-1469.

[27] J. Chen, D. Chen, Q. Chen, W. Xu, W. Zhang, W. Mu, Computer-Aided Targeted Mutagenesis of Thermoclostridium caenicola d-Allulose 3-Epimerase for Improved Thermostability, J Agric Food Chem 70(6) (2022) 1943-1951.

[28] W. Ren, L. Liu, L. Gu, W. Yan, Y.L. Feng, D. Dong, S. Wang, M. Lyu, C. Wang, Crystal Structure of GH49 Dextranase from Arthrobacter oxidans KQ11: Identification of Catalytic Base and Improvement of Thermostability Using Semirational Design Based on B-Factors, J Agric Food Chem 67(15) (2019) 4355-4366.

[29] Y. Dehouck, J.M. Kwasigroch, D. Gilis, M. Rooman, PoPMuSiC 2.1: a web server for the estimation of protein stability changes upon mutation and sequence optimality, BMC Bioinformatics 12 (2011) 151.

[30] J. Guo, Z. Rao, T. Yang, Z. Man, M. Xu, X. Zhang, S.T. Yang, Enhancement of the thermostability of Streptomyces kathirae SC-1 tyrosinase by rational design and

empirical mutation, Enzyme Microb Technol 77 (2015) 54-60.

[31] D. Zhang, X. Zhu, D. Hu, Z. Wen, C. Zhang, M. Wu, Improvement in the catalytic performance of a phenylpyruvate reductase from Lactobacillus plantarum by site-directed and saturation mutagenesis based on the computer-aided design, 3 Biotech 11(2) (2021) 69.

[32] Y. Zhu, C. Qiao, H. Li, L. Li, A. Xiao, H. Ni, Z. Jiang, Improvement thermostability of Pseudoalteromonas carrageenovora arylsulfatase by rational design, Int J Biol Macromol 108 (2018) 953-959.

[33] A. Waterhouse, M. Bertoni, S. Bienert, G. Studer, G. Tauriello, R. Gumienny, F.T. Heer, T.A.P. de Beer, C. Rempfer, L. Bordoli, R. Lepore, T. Schwede, SWISS-MODEL: homology modelling of protein structures and complexes, Nucleic Acids Res 46(W1) (2018) W296-W303.

[34] Y. Han, R. Yu, P. Gao, X. Lu, W. Yu, The hydrogen-bond network around Glu160 contributes to the structural stability of chitosanase CsnA from Renibacterium sp. QD1, Int J Biol Macromol 109 (2018) 880-887.

[35] N.T. Nguyen, T.H. Nguyen, T.N.H. Pham, N.T. Huy, M.V. Bay, M.Q. Pham, P.C. Nam, V.V. Vu, S.T. Ngo, Autodock Vina Adopts More Accurate Binding Poses but Autodock4 Forms Better Binding Affinity, J Chem Inf Model 60(1) (2020) 204-211.

[36] F. Zhu, G. Li, P. Wei, C. Song, Q. Xu, M. Ma, J. Ma, P. Song, S. Zhang, Rational engineering of a metalloprotease to enhance thermostability and activity, Enzyme Microb Technol 162 (2023) 110123.

[37] M.G. Pikkemaat, A.B. Linssen, H.J. Berendsen, D.B. Janssen, Molecular dynamics simulations as a tool for improving protein stability, Protein Eng 15(3) (2002) 185-192.

[38] L. Huang, J. Ma, J. Sang, N. Wang, S. Wang, C. Wang, H. Kang, F. Liu, F. Lu, Y. Liu, Enhancing the thermostability of phospholipase D from Streptomyces halstedii by directed evolution and elucidating the mechanism of a key amino acid residue using molecular dynamics simulation, Int J Biol Macromol 164 (2020) 3065-3074.

[39] J. Li, J. Yang, S. Mu, N. Shang, C. Liu, Y. Zhu, Y. Cai, P. Liu, J. Lin, W. Liu, Y. Sun,

Y. Ma, Efficient O-Glycosylation of Triterpenes Enabled by Protein Engineering of Plant Glycosyltransferase UGT74AC1, ACS Catalysis 10(6) (2020) 3629-3639.

[40] G. Li, X. Zhou, Z. Li, Y. Liu, D. Liu, Y. Miao, Q. Wan, R. Zhang, Significantly improving the thermostability of a hyperthermophilic GH10 family xylanase XynAF1 by semi-rational design, Appl Microbiol Biotechnol 105(11) (2021) 4561-4576.

[41] X. Jiang, Y. Wang, Y. Wang, H. Huang, Y. Bai, X. Su, J. Zhang, B. Yao, T. Tu, H. Luo, Exploiting the activity-stability trade-off of glucose oxidase from Aspergillus niger using a simple approach to calculate thermostability of mutants, Food Chem 342 (2021) 128270.

[42] M. Klaewkla, R. Pichyangkura, T. Charoenwongpaiboon, K. Wangpaiboon, S. Chunsrivirot, Computational design of oligosaccharide producing levansucrase from Bacillus licheniformis RN-01 to improve its thermostability for production of levan-type fructooligosaccharides from sucrose, Int J Biol Macromol 160 (2020) 252-263.

[43] C. Puppo, N. Chapleau, F. Speroni, M. De Lamballerie-Anton, F. Michel, C. Anon, M. Anton, Physicochemical modifications of high-pressure-treated soybean protein isolates, J Agric Food Chem 52(6) (2004) 1564-1571.

[44] Z. Xu, Y.-K. Cen, S.-P. Zou, Y.-P. Xue, Y.-G. Zheng, Recent advances in the improvement of enzyme thermostability by structure modification, Critical Reviews in Biotechnology 40(1) (2020) 83-98.

[45] Y. Wang, H. Wu, W. Zhang, W. Xu, W. Mu, Efficient control of acrylamide in French fries by an extraordinarily active and thermo-stable l-asparaginase: A lab-scale study, Food Chem 360 (2021) 130046.

[46] B. Liu, C. Zhao, Q. Xiang, N. Zhao, Y. Luo, R. Bao, Structural and biochemical studies of the glycosyltransferase Bs-YjiC from Bacillus subtilis, Int J Biol Macromol 166 (2021) 806-817.

[47] R.A. Laskowski, M.B. Swindells, LigPlot+: multiple ligand-protein interaction diagrams for drug discovery, J Chem Inf Model 51(10) (2011) 2778-2786.

[48] J. Gu, Y. Xu, Y. Nie, Role of distal sites in enzyme engineering, Biotechnology

Advances 63 (2023) 108094.

[49] S. Li, Q. Yang, B. Tang, A. Chen, Improvement of enzymatic properties of Rhizopus oryzae alpha-amylase by site-saturation mutagenesis of histidine 286, Enzyme Microb Technol 117 (2018) 96-102.

[50] A. Mishra, W.H. Khan, A.S. Rathore, Synergistic Effects of Natural Compounds Toward Inhibition of SARS-CoV-2 3CL Protease, J Chem Inf Model 61(11) (2021) 5708-5718.

[51] M.K. Scherer, B. Trendelkamp-Schroer, F. Paul, G. Perez-Hernandez, M. Hoffmann, N. Plattner, C. Wehmeyer, J.H. Prinz, F. Noe, PyEMMA 2: A Software Package for Estimation, Validation, and Analysis of Markov Models, J Chem Theory Comput 11(11) (2015) 5525-5542.

[52] Y. Wang, M. Li, W. Liang, X. Shi, J. Fan, R. Kong, Y. Liu, J. Zhang, T. Chen, S. Lu, Delineating the activation mechanism and conformational landscape of a class B G protein-coupled receptor glucagon receptor, Comput Struct Biotechnol J 20 (2022) 628-639.

[53] J. Bi, S. Chen, X. Zhao, Y. Nie, Y. Xu, Computation-aided engineering of starch-debranching pullulanase from Bacillus thermoleovorans for enhanced thermostability, Appl Microbiol Biotechnol 104(17) (2020) 7551-7562.

[54] H.B.L. Jones, S.A. Wells, E.J. Prentice, A. Kwok, L.L. Liang, V.L. Arcus, C.R. Pudney, A complete thermodynamic analysis of enzyme turnover links the free energy landscape to enzyme catalysis, FEBS J 284(17) (2017) 2829-2842.

[55] P. Sang, S.Q. Liu, L.Q. Yang, New Insight into Mechanisms of Protein Adaptation to High Temperatures: A Comparative Molecular Dynamics Simulation Study of Thermophilic and Mesophilic Subtilisin-Like Serine Proteases, Int J Mol Sci 21(9) (2020) 3128.

[56] K.A. Konovalov, I.C. Unarta, S. Cao, E.C. Goonetilleke, X. Huang, Markov State Models to Study the Functional Dynamics of Proteins in the Wake of Machine Learning, JACS Au 1(9) (2021) 1330-1341.

[57] J. Weiser, P.S. Shenkin, W.C. Still, Approximate atomic surfaces from linear combinations of pairwise overlaps (LCPO), Journal of Computational Chemistry 20(2) (1999) 217-230.

[58] V. Kumar, P. Pandey, D. Idrees, A. Prakash, A.M. Lynn, Delineating the effect of mutations on the conformational dynamics of N-terminal domain of TDP-43, Biophys Chem 250 (2019) 106174.

[59] M.A. Maria-Solano, T. Kinateder, J. Iglesias-Fernandez, R. Sterner, S. Osuna, In Silico Identification and Experimental Validation of Distal Activity-Enhancing Mutations in Tryptophan Synthase, ACS Catal 11(21) (2021) 13733-13743.

[60] X. Wang, X. Zhang, C. Peng, Y. Shi, H. Li, Z. Xu, W. Zhu, D3DistalMutation: a Database to Explore the Effect of Distal Mutations on Enzyme Activity, J Chem Inf Model 61(5) (2021) 2499-2508.

[61] S. Salar, F. Mehrnejad, R.H. Sajedi, J.M. Arough, Chitosan nanoparticles-trypsin interactions: Bio-physicochemical and molecular dynamics simulation studies, Int J Biol Macromol 103 (2017) 902-909.

[62] A. Roy, S. Ray, Exploring RNA-protein interaction between two mesophilic bacteria: an in silico approach to discern detailed molecular level interaction in cold shock response, Biologia (2023) 1-14.

[63] A. Subramanian, P. Kadirvel, S. Anishetty, Insights into the pH-dependent catalytic mechanism of Sulfolobus solfataricus beta-glycosidase: A molecular dynamics study, Carbohydr Res 480 (2019) 42-53.

[64] Z. Chen, Y. Fu, W. Xu, M. Li, Molecular Dynamics Simulation of Barnase: Contribution of Noncovalent Intramolecular Interaction to Thermostability, Mathematical Problems in Engineering 2013 (2013) 1-12.

[65] L. Liu, L. Cai, Y. Chu, M. Zhang, Thermostability mechanisms of beta-agarase by analyzing its structure through molecular dynamics simulation, AMB Express 12(1) (2022) 50.

[66] M. Arnittali, A.N. Rissanou, M. Amprazi, M. Kokkinidis, V. Harmandaris, Structure

and Thermal Stability of wtRop and RM6 Proteins through All-Atom Molecular Dynamics Simulations and Experiments, Int J Mol Sci 22(11) (2021) 5931.

Figure Captions

Figure 1. Effects of site mutation on BS-YjiC enzyme activities. (a) Initial activities of WT and its enzyme variants. Enzyme activities of WT were defined as 100%. (b) Residual activities of enzyme variants after incubation at 45 °C for 90 min. Enzymatic activities without heat treatment were defined as 100%. The data present mean ± S.D. for three biological replicates, and the significant difference was analyzed by one-way ANOVA followed by t test. All data were statistically analyzed using GraphPad Prism 8.0. "*" present $p<0.05$, "**" present $p<0.01$, "***" present $p<0.001$.

Figure 2. Residual enzymatic activities of the WT and variants after heating at 45 ℃ for 30, 60 and 90 min. Initial enzymatic activities for all enzymes were defined as 100%. Each experiment had three replicates.

Figure 3. Surface hydrophobicity for variant K125I/N178I and the WT.

Figure 4. Analysis of variant K125I/N178I and the WT using the ProtScale online software. (a) Hydrophobicity and (b) Flexibility.

Figure 5. Docking results of glycosyltransferase BS-YjiC (PDB ID: 6KQX) with protopanaxadiol (PPD) and processed by PyMol. Cyan sticks represent positions of point mutation of Lys125 and Asn178. Blue and magenta colors represent PPD and UDP, respectively. Red and yellow colors represent α-helices and β-sheets, respectively. Green color represents loops and other secondary structures.

Figure 6. Superimposed diagram of interactions between variant K125I/N178I and the WT. (a) Ginsenoside PPD binding site. (b) UDP binding site. (c) Residue Ile125 sites.

(d) Residue Ile178 sites. Automatic superimposed by LigPlot+, and the WT plot was automatically fitted to the K125I/N178I map. Red circles and ellipses identify the equivalent residues in the two 3D structures. Hydrogen bonds are shown as green dashed lines, while the spoke arcs indicate residues undergoing hydrophobic interactions forces with the ligand.

Figure 7. MD simulation analysis of enzyme protein before and after mutation. (A) Residue dynamic cross-correlation matrix and (B) Free Energy Landscape (FEL). (a) Pure protei, (b) WT-ligand complex, (c) Variant-ligand complex.

Figure 8. Functional conformational changes elucidated by MSMs.

Figure 9. Solvent-accessibility surface area (SASA) for WT, K125I, K125I/N178I and M315F at different temperatures. (a) 308 K, (b) 400 K, (c) 440 K, (d) 480 K.

Figure 10. Root Mean Square Deviation (RMSD) for WT, K125I, K125I/N178I and M315F at different temperatures. (a) 308 K, (b) 400 K, (c) 440 K, (d) 480 K.

Figure 11. Root Mean Square Fluctuation (RMSF) for WT, K125I, K125I/N178I and M315F at different temperatures. (a) 308 K, (b) 400 K, (c) 440 K, (d) 480 K.

Figure 12. Optimization of conditions for cascade reactions of variant K125I/N178I/AtSuSy.

Figure 13. The fed-batch reaction system for synthesizing ginsenosides Rh2 and F12. PPD (1 mM) was added to the reaction system at 1, 2, 4, 6, 8 and 10 h. Fresh enzymes (100 mU/mL Bs-YjiC and 240 mU/mL AtSuSy) were added at 4 and 8 h (pH 8.0; and temperature 45 ℃).

Table 1. Kinetic characteristics for WT and glycosyltransferase variants

enzyme	T_{opt}[a] (℃)	T_m (℃)	K_m (μM)	V_{max} (U/mg)	k_{cat} (s^{-1})	k_{cat}/K_m (s^{-1} M^{-1})	refs
WT	40	47.30	131.90 ± 32.12	8.32± 0.36	0.96 ± 0.06	0.72× 10^4	Ts[b]
K125I	40	51.08	127.90 ± 22.4	8.60 ± 0.41	0.99 ± 0.05	0.77× 10^4	Ts
N178I	40	48.28	132.30 ± 33.82	8.75 ± 0.62	1.01 ± 0.07	0.76× 10^4	Ts
P313W	40	50.04	136.40 ± 32	8.94 ± 0.60	1.11 ± 0.08	0.81× 10^4	Ts
K125I/N178I	45	54.51	116.90 ± 22.49	8.82 ± 0.45	1.01 ± 0.05	0.87× 10^4	Ts
K125I/P313W	45	53.07	120.80 ± 23.11	8.56 ± 0.44	0.98 ± 0.05	0.82× 10^4	Ts
Bs-YjiC	40	ND[c]	163.00 ± 16.76	11.40 ± 0.39	1.31 ± 0.04	0.34 × 10^4	[15]
M315F	35	ND	ND	ND	ND	ND	[17]

a Opt.: Optimum temperature. b Ts: This study. c ND: Not detected.

Table 2. Optimization of the ratio of variant enzymes K125I/N178I and AtSuSy in the reaction cascade

Entry	K125I/N178I (mU/mL)	AtSuSy (mU/mL)	Conversion rate of PPD (%)	F12 (mM)	Rh2 (mM)
1	50	300	43%	0.40	0.03
2	100	300	64%	0.60	0.04
3	200	300	69%	0.65	0.04
4	300	300	72%	0.68	0.04
5	100	60	25%	0.12	0.13
6	100	120	58%	0.43	0.15
7	100	240	71%	0.67	0.04
8	100	360	73%	0.69	0.04

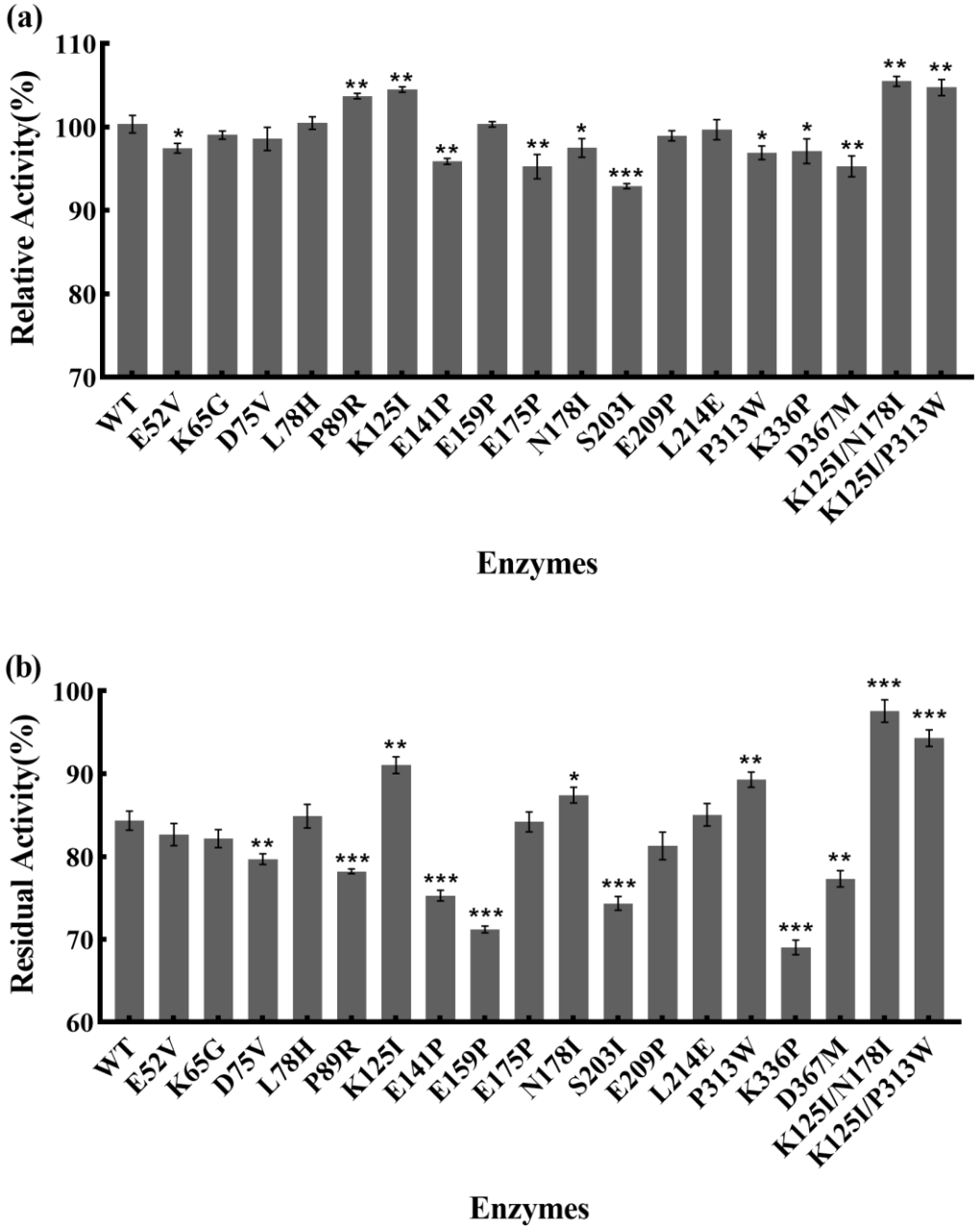

Figure 1. Effects of site mutation on BS-YjiC enzyme activities. (a) Initial activities of the WT and its enzyme variants. Enzyme activities of wild type (WT) were defined as 100%. (b) Residual activities of enzyme variants after incubation at 45 °C for 90 min. Enzymatic activities without heat treatment were defined as 100%. The data present mean ± S.D. for three biological replicates, and the significant difference was analyzed by one-way ANOVA followed by t test. All data were statistically analyzed

using GraphPad Prism 8.0. “*” present $p<0.05$, “**” present $p<0.01$, “***” present $p<0.001$.

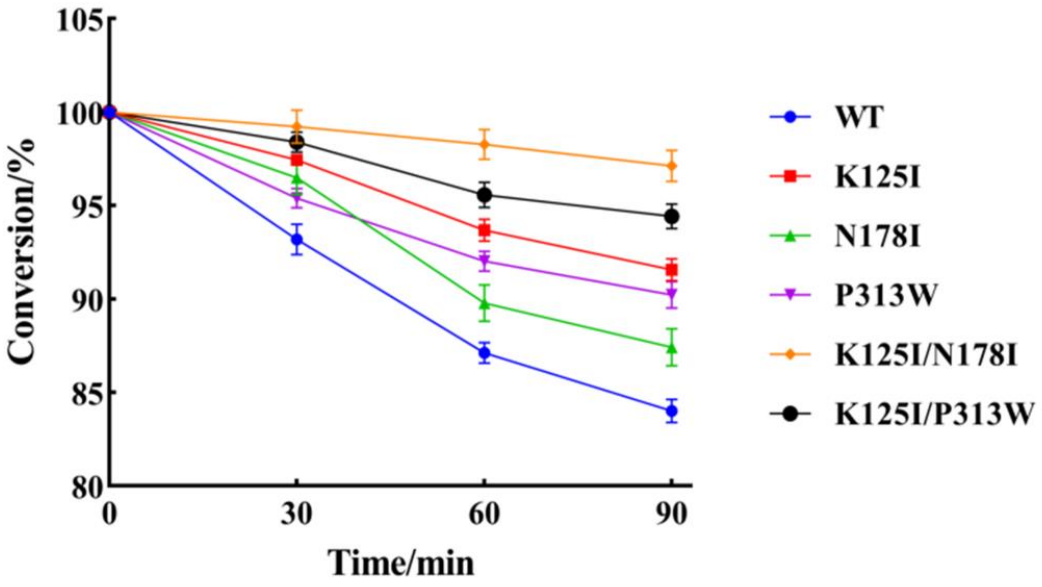

Figure 2. Residual enzymatic activities of the WT and variants after heating at 45 ℃ for 30, 60 and 90 min. Initial enzymatic activities for all enzymes were defined as 100%. Each experiment had three replicates.

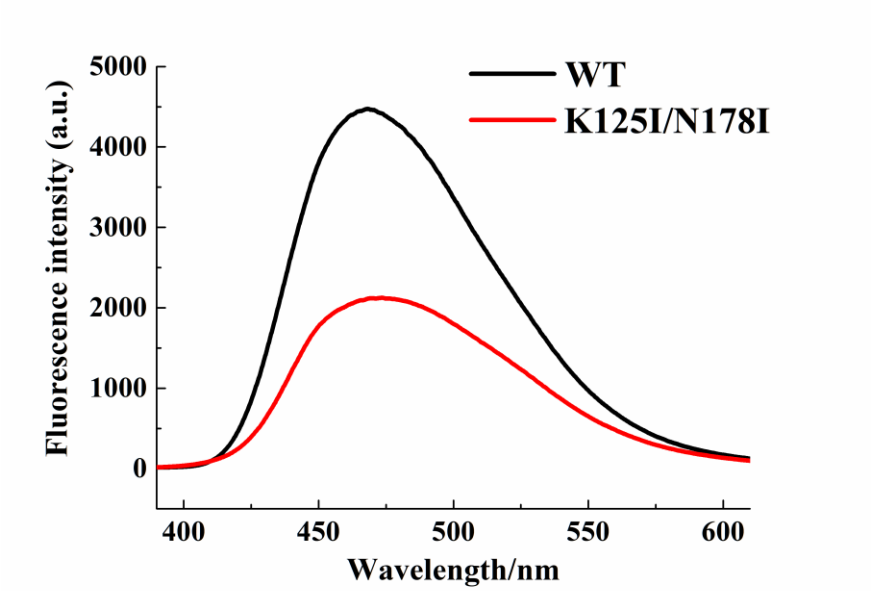

Figure 3. Surface hydrophobicities for variant K125I/N178I and the WT.

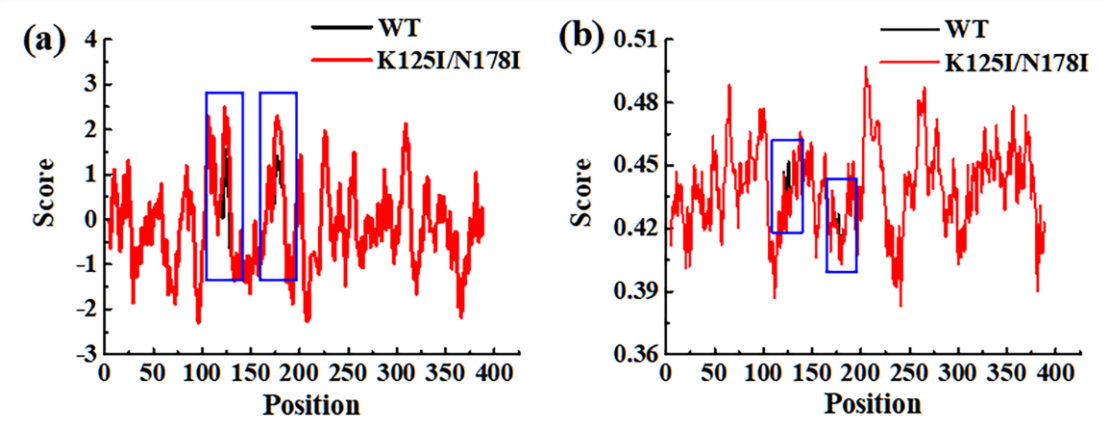

Figure 4. Analysis of variant K125I/N178I and WT by the online software ProtScale.

(a) Hydrophobicity and (b) flexibility.

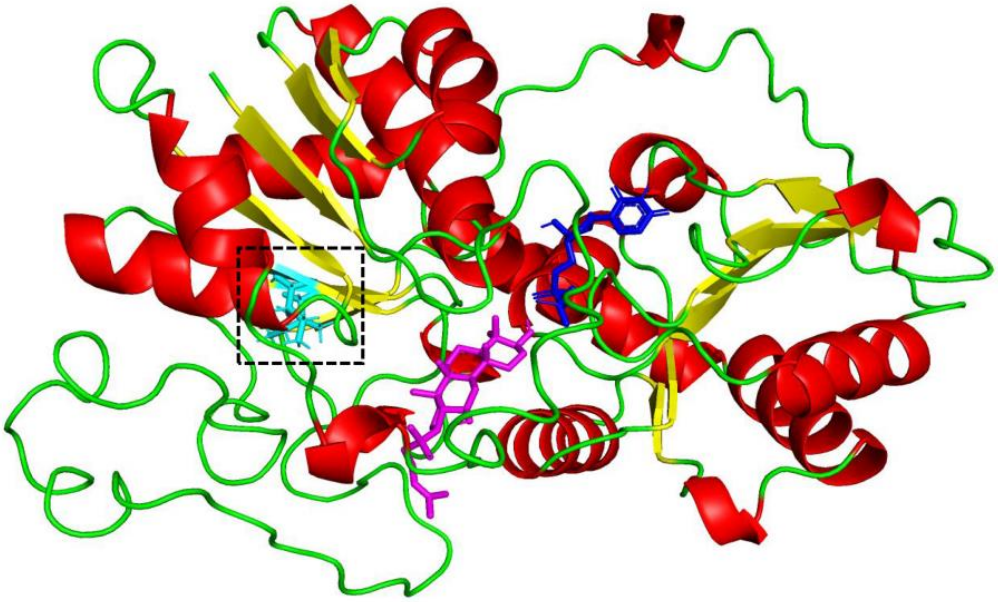

Figure 5. Docking results of glycosyltransferase BS-YjiC (PDB ID: 6KQX) with protopanaxadiol (PPD) as processed by PyMol. Cyan sticks represent positions of point mutations of Lys125 and Asn178. Blue and magenta colors represent PPD and UDP, respectively. Red and yellow colors represent α-helices and β-sheets, respectively. The green color represents loops and other secondary structures.

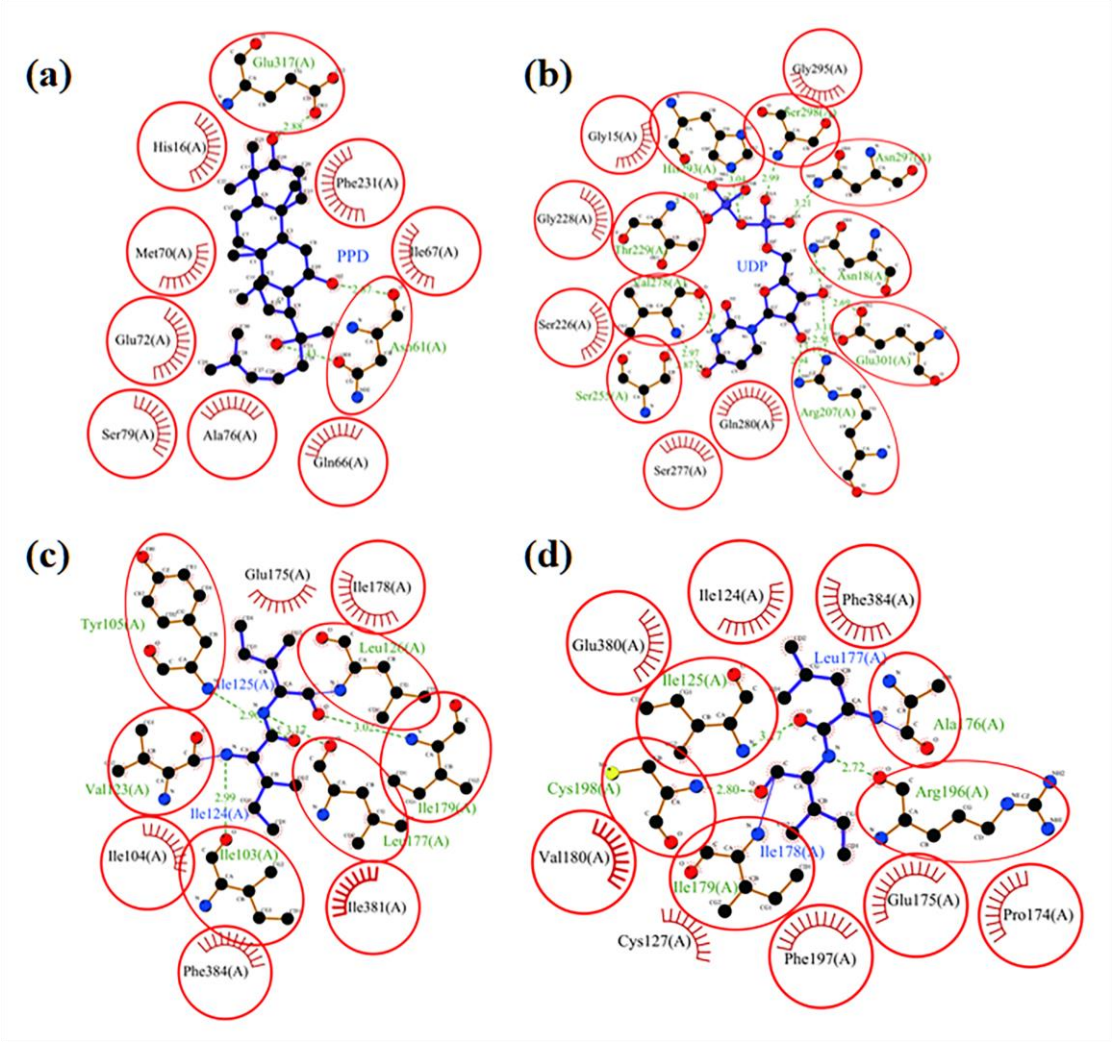

Figure 6. Superimposed diagram of interactions between variant K125I/N178I and the WT. (a) Ginsenoside PPD binding site. (b) UDP binding site. (c) Residue Ile125 sites. (d) Residue Ile178 sites. Automatic superimposed by LigPlot+. The WT plot was automatically fitted to the K125I/N178I map. Red circles and ellipses identify the equivalent residues in two 3D structures. Hydrogen bonds are shown as green dashed lines while spoke arcs indicate residues undergoing hydrophobic interaction forces with the ligand.

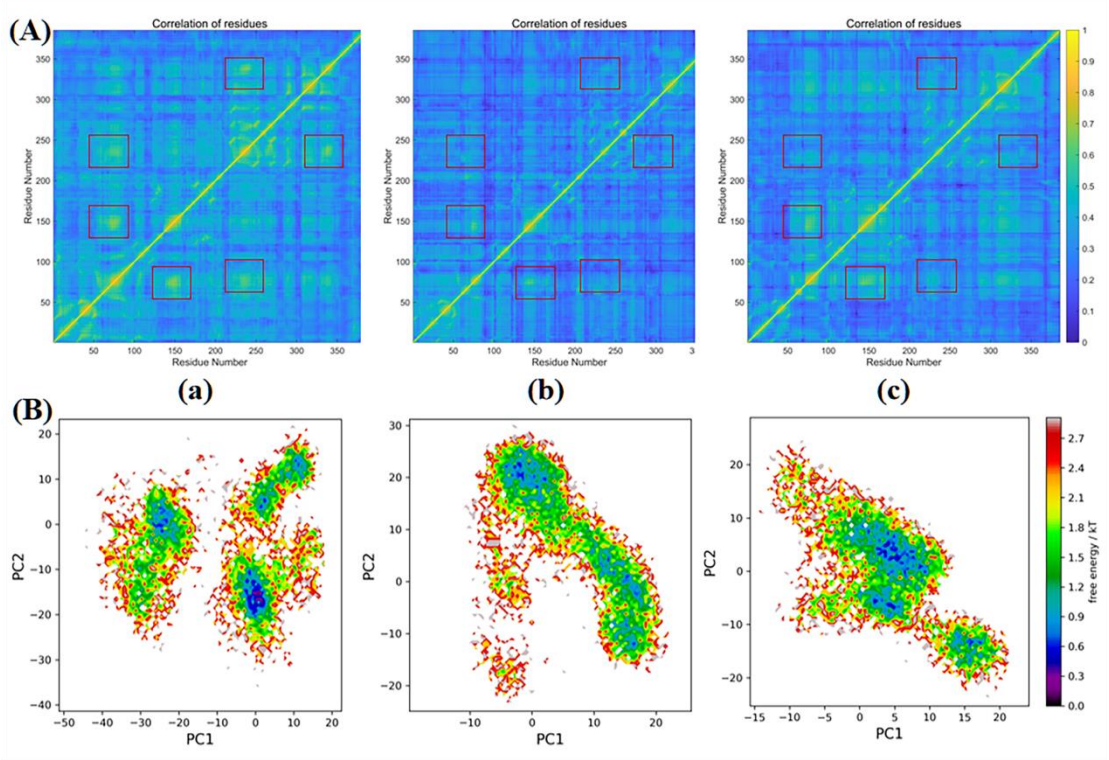

Figure 7. MD simulation analysis of enzyme protein before and after mutation. (A) Residue dynamic cross-correlation matrix and (B) Free Energy Landscape (FEL). (a) Pure protei, (b) WT-ligand complex, (c) Variant-ligand complex.

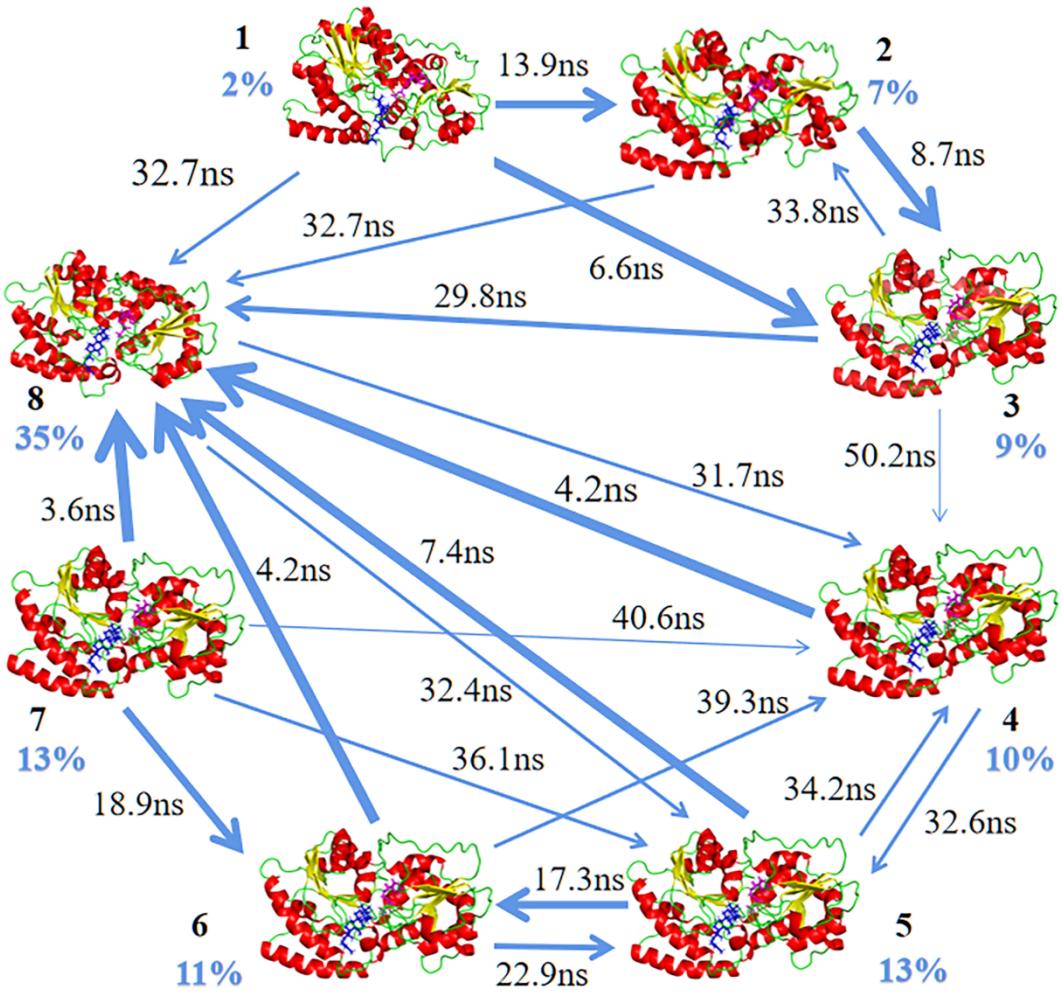

Figure 8. Functional conformational changes as elucidated by MSMs.

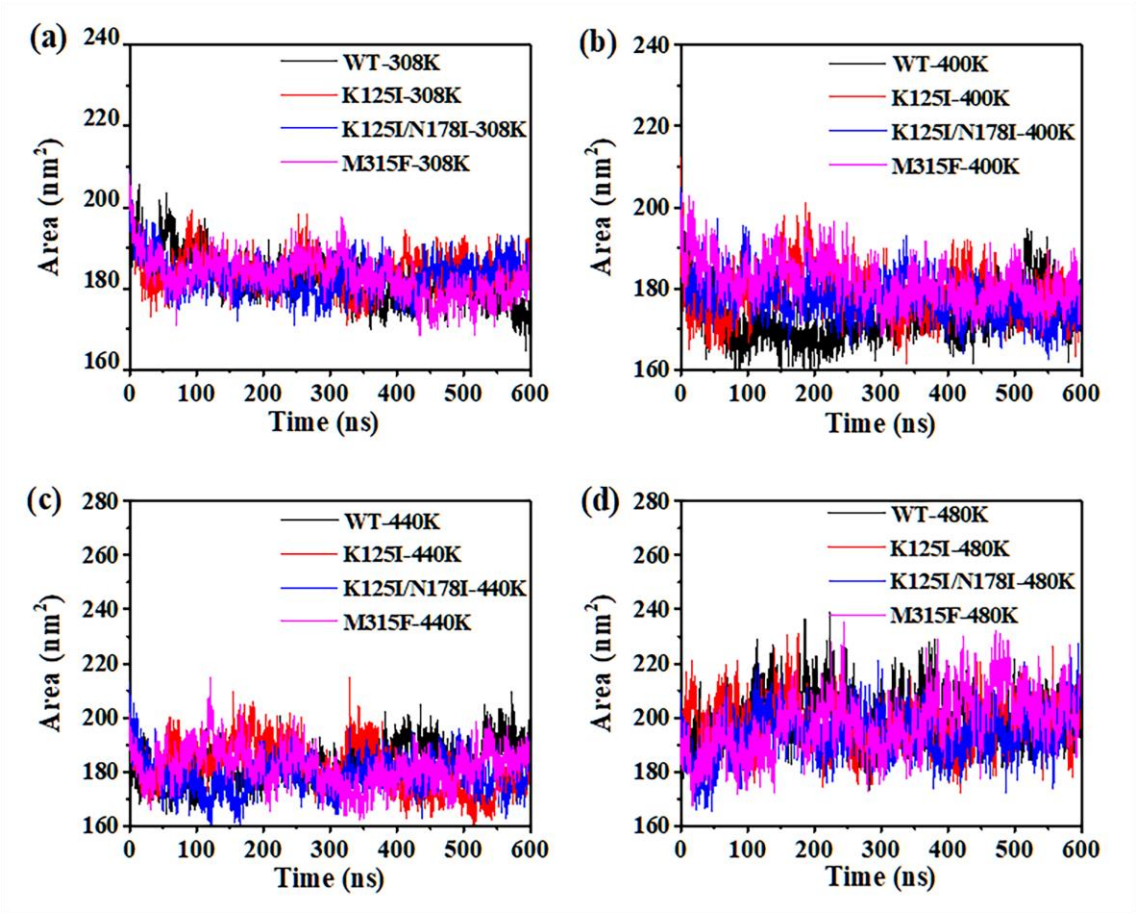

Figure 9. Solvent-accessibility surface area (SASA) for WT, K125I, K125I/N178I and M315F at different temperatures. (a) 308 K, (b) 400 K, (c) 440 K, (d) 480 K.

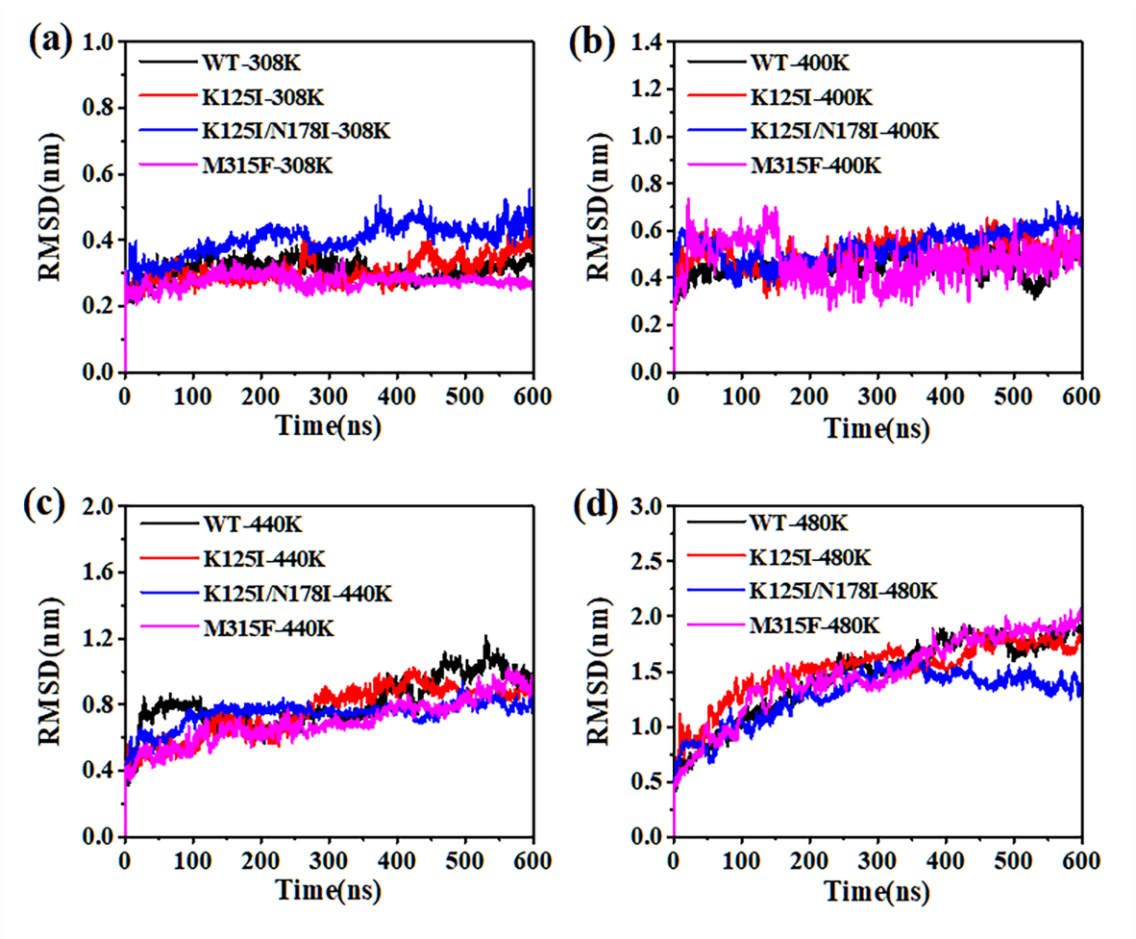

Figure 10. Root Mean Square Deviation (RMSD) for WT, K125I, K125I/N178I and M315F at different temperatures. (a) 308 K, (`b) 400 K, (c) 440 K, (d) 480 K.

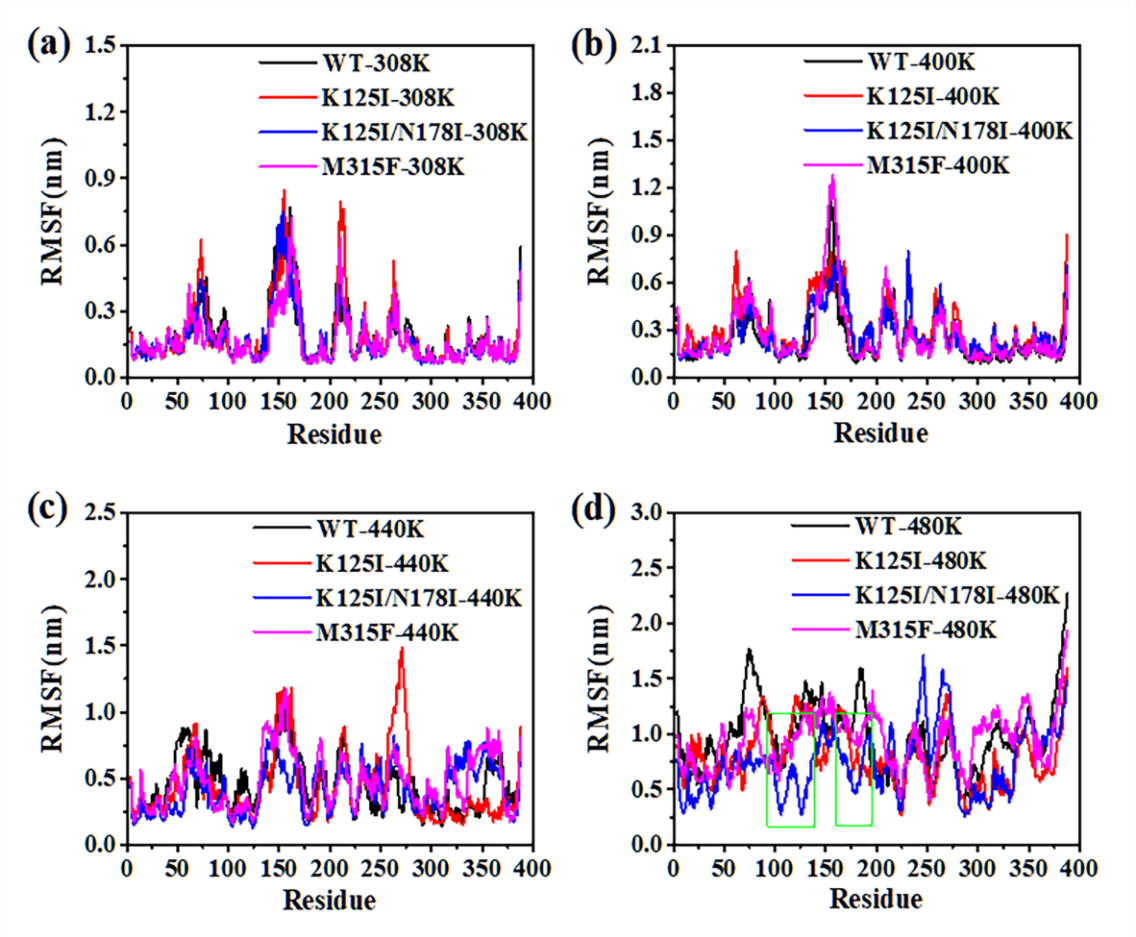

Figure 11. Root Mean Square Fluctuation (RMSF) for WT, K125I, K125I/N178I and M315F at different temperatures. (a) 308 K, (b) 400 K, (c) 440 K, (d) 480 K.

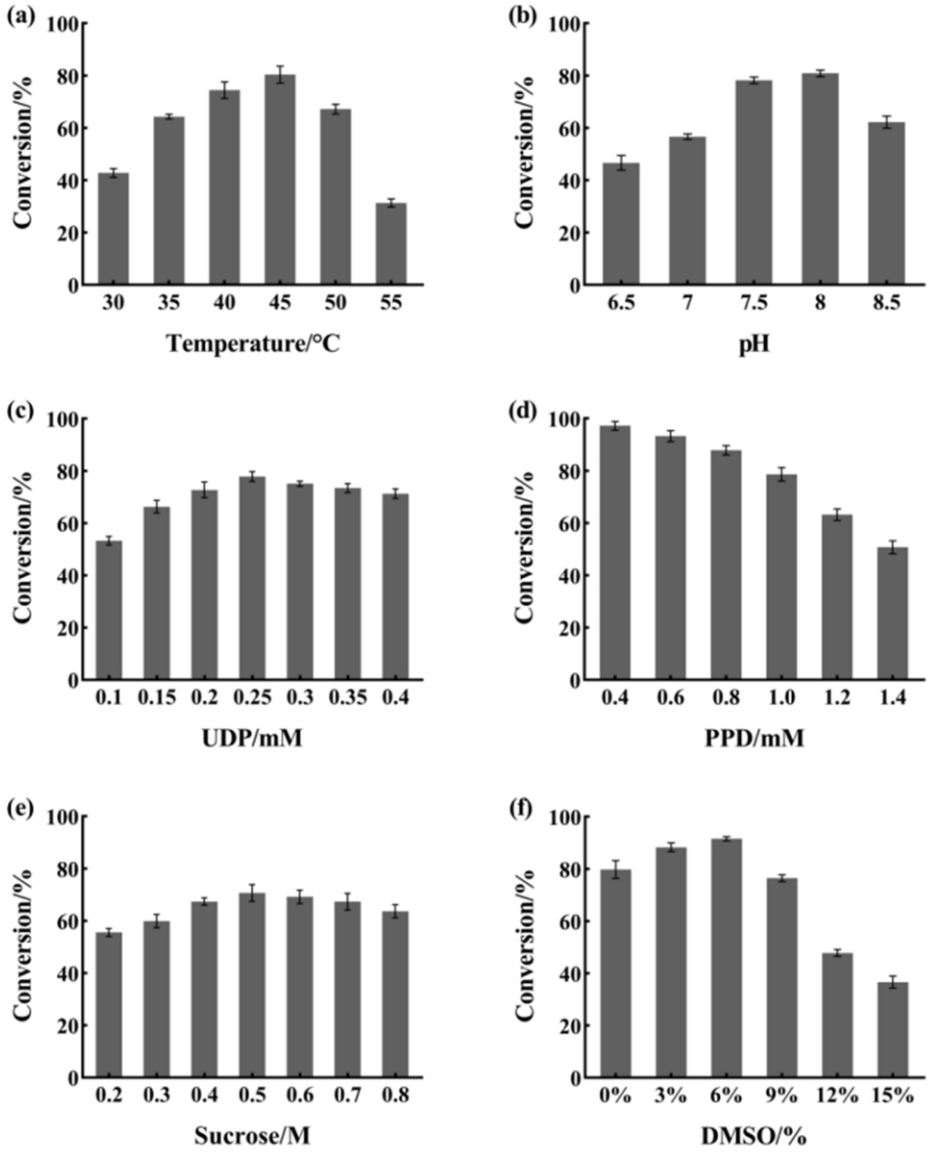

Figure 12. Optimization of cascade reaction conditions for variant K125I/N178I/AtSuSy.

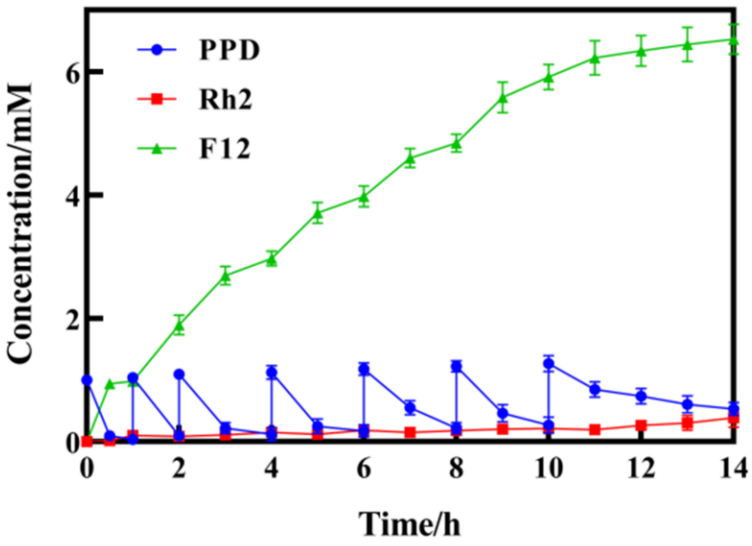

Figure 13. The fed-batch reaction system for synthesizing ginsenosides Rh2 and F12. PPD (1 mM) was added to the reaction system at 1, 2, 4, 6, 8 and 10 h. Fresh enzymes (100 mU/mL Bs-YjiC and 240 mU/mL AtSuSy) were added at 4 and 8 h (pH 8.0; and temperature 45 ℃).